Iraqi Journal for Computer Science and Mathematics

Manuscript 1273

Enhancing Image Denoising Performance through Cosine Similarity-Based Block Matching and Adaptive Thresholding - CA-EBM3D

R. Padmapriya

A. Jeyasekar

IRAQI JOURNAL FOR COMPUTER SCIENCE AND MATHEMATICS 2025;6:93–108

ORIGINAL STUDY

Enhancing Image Denoising Performance through Cosine Similarity-Based Block Matching and Adaptive Thresholding - CA-EBM3D

R. Padmapriya *, **A. Jeyasekar**

Department of Computing Technologies, School of Computing, SRM Institute of Science and Technology, Kattankulathur, Chennai, Tamil Nadu 603203, India

ABSTRACT

Image denoising plays a vital role in enhancing visual quality by effectively suppressing noise while retaining critical image structures and textures. Traditional Block-Matching and 3D (BM3D) Filtering techniques, although widely adopted, often encounter challenges in achieving an optimal trade-off between noise reduction and feature preservation due to limitations in fixed-thresholding strategies and suboptimal block matching. To address these shortcomings, this study introduces a novel Cosine Adaptive BM3D (CA-BM3D) approach, which integrates cosine similarity for more accurate block matching and incorporates adaptive thresholding to enhance denoising efficiency. The proposed method was evaluated on six standard 8-bit grayscale images such as Leena (512*512), Barbara (512*512), Zelda (512*512), peppers (512*512), Cameraman (512*512), House (512*512) contaminated with Additive White Gaussian Noise (AWGN) Results demonstrate that the Cosine Adaptive BM3D algorithm consistently outperforms conventional BM3D across all test cases, achieving an average PSNR of 31.28 dB and SSIM of 0.678. Notably, for the "Leena" image, the cosine-based approach attained a PSNR of 31.42 dB and SSIM of 0.8921, surpassing alternative distance metrics such as Euclidean (30.55 dB, 0.8782), Manhattan (29.96 dB, 0.8657), Jaccard (28.78 dB, 0.8425), and Minkowski (30.02 dB, 0.8691). Similar performance gains were observed for the other images: "Barbara" (30.33 dB, 0.8856), "Zelda" (32.15 dB, 0.9012), "Peppers" (31.78 dB, 0.8967), "Cameraman" (30.02 dB, 0.8823), and "House" (32.89 dB, 0.9105). These findings substantiate the effectiveness of the cosine similarity measure in enhancing both noise suppression and structural fidelity in the denoising process.

Keywords: Image processing, Filtering, Block matching, Cosine-based similarity, Image denoising, Soft thresholding

1. Introduction

Image denoising is an indispensable preprocessing task in digital image processing, crucial for enhancing the quality of visual data by mitigating noise while preserving essential image details such as edges and textures [1, 2]. Various denoising techniques have been developed over the years, spanning spatial domain filters and frequency domain approaches, each with specific strengths and limitations. More advanced algorithms, such as Non-Local Means (NLM) and Block-Matching and 3D Filtering (BM3D), have demonstrated superior performance by leveraging patch redundancy and collaborative filtering mechanisms [3]. However, these methods often encounter challenges when processing high-resolution images or data corrupted by strong noise such as additive white Gaussian noise (AWGN), where distinguishing between noise and fine image structures becomes increasingly complex.

Despite these advancements, existing techniques often struggle to maintain a balance between effective noise reduction and the preservation of fine image details. A significant limitation lies in the block

Received 12 November 2024; revised 28 April 2025; accepted 4 May 2025.
Available online 4 July 2025

* Corresponding author.
E-mail addresses: Pr1836@srmist.edu.in (R. Padmapriya), jeyaseka@srmist.edu.in (A. Jeyasekar).

https://doi.org/10.52866/2788-7421.1273

matching stage of patch-based methods, which typically utilize Euclidean distance to measure similarity between blocks. While Euclidean distance is effective in certain contexts, it becomes less reliable in high-dimensional noisy environments [4, 5]. It is sensitive to variations in pixel intensity that may arise from brightness or contrast fluctuations rather than genuine structural differences. Consequently, this leads to inaccurate grouping of similar patches, which in turn undermines the effectiveness of collaborative filtering and denoising performance.

To address this issue, this study proposes a modification to the conventional BM3D approach by incorporating cosine similarity as the similarity metric during the block matching phase [6, 7]. Unlike Euclidean distance, cosine similarity evaluates the angular similarity between vectors, focusing on their orientation rather than magnitude. This makes it inherently more robust to brightness variations and intensity shifts, which are typical distortions introduced by AWGN [8]. By prioritizing the structural orientation of pixel patterns, cosine similarity ensures that only truly similar patches are grouped together, thus improving the accuracy of the filtering process and preserving intricate image features more effectively.

The motivation for adopting cosine similarity is further supported by its successful application in various domains involving high-dimensional data, such as text mining, face recognition, and content-based image retrieval. Studies have shown that cosine-based measures are particularly advantageous when the relative arrangement of features is more informative than their absolute values [9]. Extending this principle to image denoising, especially under conditions of AWGN corruption, provides a strong theoretical foundation for the proposed enhancement. This approach not only strengthens the robustness of the denoising algorithm but also maintains computational efficiency comparable to existing BM3D methods.

This modification has significant implications for real-world applications where image quality is paramount. In medical imaging, improved denoising translates to clearer visualization of anatomical structures in MRI, CT, or ultrasound scans, supporting more accurate diagnosis and clinical decisions [10]. In satellite imaging, where images are susceptible to atmospheric noise and sensor errors, the proposed approach enhances landform recognition and object detection by preserving edge fidelity. Similarly, in industrial inspection and low-light surveillance, the ability to maintain structural integrity in noisy environments enhances reliability in visual analysis tasks. Therefore, this research contributes not only a technical improvement to an established algorithm but also addresses practical challenges in diverse application domains requiring high-fidelity image reconstruction.

This paper is organized as follows: Section 2 reviews the related work regarding the existing methods for image denoising, from basic filtering techniques and algorithms to some other recent developments comprising the spatial and frequency domains, nonlocal means, and BM3D filtering. It proposes, in Section 3, a denoising model. Further, the details are given regarding the architecture of the model, methodology behind it, and the novelties it introduces toward an effective AWGN removal problem with image details preservation. Section 4 presents an extended performance study by analyzing the results provided by the proposed model and comparing them with other methods currently representing the state of the art in terms of denoising quality, quality metrics evaluation, and computation efficiency. Finally, Section 5 concludes the paper summarizing the contributions made by restating the key results obtained and outlining a possible future research direction toward further advances in image denoising techniques.

2. Novelty and contributions of the proposed research

The following are some of the novelty and contributions of the proposed research:

- ***Integration of Cosine Similarity into BM3D Block Matching:*** Unlike conventional BM3D and its variants that rely on Euclidean distance for block similarity, the proposed method incorporates cosine similarity to enhance the accuracy of patch grouping. This addresses a core limitation in standard BM3D, its sensitivity to intensity variation by measuring angular similarity rather than magnitude differences, thus better preserving structural features in high-noise settings.
- ***Customized Adaptive Thresholding Mechanism:*** Adaptive thresholding is not novel in itself; however, the implementation in this research is tailored to the cosine similarity framework**.** Instead of relying on fixed or statistically derived global thresholds, the proposed method employs a locally adaptive thresholding scheme that dynamically adjusts based on the cosine similarity values between blocks. This ensures that only structurally aligned patches are selected for collaborative filtering, thereby improving denoising efficiency and fidelity.
- ***Preservation of Fine Structural Details in High-Noise Scenarios:*** The synergy of cosine-based block matching and adaptive thresholding

facilitates superior edge and texture preservation, even under high-intensity additive white Gaussian noise. This is particularly advantageous over earlier BM3D modifications, which either enhance noise suppression at the cost of detail loss or require extensive parameter tuning.

- ***Balanced Alternative to Deep Learning-Based Denoising Methods:*** While deep learning approaches (e.g., DnCNN, FFDNet, and Noise2Void) achieve impressive denoising results, they demand large-scale training datasets, significant computational resources, and often generalize poorly across unseen noise types or imaging conditions. In contrast, the proposed method is data-independent, does not require retraining, and performs robustly across varying noise levels by making it highly suitable for real-time or low-resource environments such as satellite imaging and embedded medical devices.
- ***Enhanced Practical Applicability across Critical Domains:*** The proposed improvements are directly beneficial for real-world applications such as medical imaging, where preserving fine details is critical for diagnostics; satellite imaging, where noise from transmission and sensors must be addressed; and low-light surveillance, where structural clarity enhances scene understanding. These domains demand denoising methods that combine accuracy, robustness, and computational efficiency, all of which are achieved in the proposed framework.

3. Related works

Image denoising has become important over the years because of its relevance in the enhancement of image quality with regard to various types of noise. Many techniques have been proposed throughout the years to serve this purpose, with the attempt of removing noise while preserving the integrity of features related to edges, textures, and fine details in the images. The traditional approaches have filters in the spatial domain, like mean, median, and Gaussian filters, which works directly on the pixel intensities. Though this method is effective for specific types of noise, these techniques needs more improvement in noise reduction and details preservation.

Dabov et al. [11] proposed an integrated BM3D combining principal component analysis with BM3D. The work has been extended to denoising color images and videos. However, this algorithm requires careful tuning of model parameters for improving the results. Hasan and E-Sakka [12] deployed Structural similarity to be used in the wiener filter in BM3D. This filtering effectively preserves the image quality and structural details. However, it cannot handle diverse types of noises added to the images. Knaus and Zwicker [13] took initiatives in developing a new version of BM3D by improving filtering in BM3D. They proposed a denoising method with dual domains such as transform and spatial domain. These denoising methods apply non-local and bilateral filters to the spatial domain. Although this algorithm preserves the high contrast image features, low-contrast details fail to be preserved. Ali Abdullah Yahya et al. [14] presented a modified BM3D algorithm that replaces the conventional hard thresholding with the adaptive filtering methodology. This enables the system to adapt and proceed with changes per the input signal variation. In addition, this study also used a k-means clustering algorithm to divide the image into several regions and detect the boundaries between these regions. This process reduces the risk of estimating poor matching. Finally, the results are determined using visual quality, structural similarity index, and peak signal-to-noise ratio. However, this strategy faces issues like parameter sensitivity.

Rui Chen et al. [15] developed an image-denoising technique named improved K-singular value decomposition (K-SVD) and dictionary atom optimization. This study addresses the drawback of the conventional K-SVD approach under strong noise. Initially, a correlation coefficient-matching condition was employed to estimate a sparse representation of the image dictionary. Then, the dictionary noise atom was identified and removed based on the noise intensity and structural complexity. The experimental results depict that this strategy enhances the smoothness of homogeneous regions while preserving the texture and edge of the image. Rejeesh M R and Thejaswini P [16] proposed an innovative denoising algorithm based on optimal trilateral filtering. This algorithm utilized grey wolf optimization to optimize the trilateral filtering. Initially, a noisy image database was created by adding different noises, such as random, Gaussian, and Salt and Pepper noise. Consequently, the noisy images are filtered through the BM3D technique. Further, optimal trilateral filtering was used to reconstruct the denoised images. This strategy employs two-level filtering, like moving frame-based BM3D and optimal trilateral filtering. The implementation showed that this strategy offered better mean square error and peak signal-to-noise ratio results. However, this strategy is prone to computational overhead.

Generally, conventional image denoising strategies have good interpretability, but they face issues with optimal denoising results. Hence, Zhe Li et al. [17] developed a hybrid image denoising framework

by combining the traditional BM3D, weighted kernel norm minimization, and non-subsampled shearlet transform. The input images are denoised using these techniques, increasing texture information extraction. Consequently, an adaptive thresholding approach was employed to address the discontinuity of the hard thresholding variations. The implementation outcomes of this algorithm highlighted that it achieved better results in terms of peak signal-to-noise ratio. However, this methodology is resource-intensive, and implementation is costly. Huakun Huang et al. [18] presented a study to develop an image-denoising mechanism for medical image analysis. This study proposed a self-supervised sparse coding strategy for removing the noise features from the medical images. This algorithm does not depend on the ground truth image of the noisy and clean images to differentiate the noise features. This algorithm also creates the deep neural network (DNN) to ensure adaptability in analyzing the changing characteristics of the input images. The implementation outcomes demonstrated that this strategy obtained a reduced error rate compared to conventional algorithms. However, this algorithm offers limited scalability, which limits its application in real-world scenarios.

Hu Deng et al. [19] proposed an image-denoising framework for ultrasonic logging images. This study aims to remove noise features under strong noise conditions. Initially, a sparse coefficient is simulated by a highly effective Laplacian distribution. Subsequently, a dynamic Bayesian denoising strategy was utilized as a prior term of sparse coefficients. Finally, semi-quadratic regularization was employed to reduce the complexity of the process. In addition, a relaxation parameter was introduced to increase the model's accuracy. The simulation showed that this hybrid strategy obtained improved denoising results compared to the conventional algorithms. However, this strategy consumes more computational time than others. To overcome the drawbacks of the BM3D filters, in this paper, we replace the steady-state hard thresholding process with adaptive filtering. Soft thresholding is an alternative to hard thresholding in adaptive filtering. Image areas with high noise are concentrated and reduced or removed, thus making the image clearer. Distance calculation is one of the most important aspects of grouping, and we introduce cosine distance by replacing Euclidean distance. Cosine similarity measures provide a more accurate way of finding and grouping similar blocks for further aggregation.

Nevertheless, there are still different research gaps that denote further investigation and improvement for de-noising techniques [20]. Some important lacunas involve reliance on traditional metrics of evaluation such as PSNR and SSIM to assess the performance of image de-noising techniques. While these metrics provide quantifiable measures of image quality, they do not fully encapsulate the perceptual quality or visual fidelity of the denoised images. There is, therefore, an urgent need for more holistic evaluations that also include human visual perception models and other relevant metrics to give a full understanding of the effectiveness of denoising algorithms. Secondly, most existing algorithms, including BM3D, tend to have poor performance at higher noise levels. Most of these techniques do wonders at low noise but start to degrade in efficiency as the noise becomes intensive. Under these noisy conditions, images suffer a great loss of detail and structural integrity [21, 22]. In this regard, future research directions should be geared toward the realization of robust denoising algorithms that can efficiently handle a variety of noise types, especially those under adverse conditions, such as in low-light conditions or when processing images acquired in the presence of multiple noise sources.

Another literature gap [23, 24] involves the challenge of preserving salient image features while removing noise. In regard to image denoising, most of the algorithms created to handle such tasks inadvertently make the edges, textures, and fine details blurred, which is very prejudicial to the quality of the denoised image. This issue gives rise to the need for novel approaches that can excel not only in noise reduction but also in the preservation of salient features. Besides, the integration of modern techniques, such as machine learning and deep learning, into algorithms of denoising has not been explored yet. Tapping into such technologies, it is envisioned that heavy lifting of performance can be achieved by making adaptive or context-aware processing dependent on the characteristics of the noise and image content [25]. The addressing of these gaps may eventually pay off with the development of effective and versatile methods for image denoising and, by that virtue, advance the field of digital image processing.

4. Proposed methodology

In this paper, an enhanced image denoising method called CA-BM3D (Cosine Adaptive BM3D approach), which addresses key limitations of the conventional BM3D algorithm is proposed. BM3D is a well-established state-of-the-art denoising technique that relies on block-matching and collaborative 3D filtering. The BM3D algorithm operates in two main stages: basic estimation and final estimation. In the basic stage, blocks of similar patches are subjected to a 3D transform and hard thresholding to produce a preliminary denoised image. This initial estimate

Table 1. Comparison between BM3D and CA-BM3D BM3D in terms of block matching, thresholding, and final reconstruction.

Feature	BM3D (Baseline)	CA-BM3D (Proposed)
Block Matching	Uses Euclidean Distance to measure similarity between blocks	Uses Cosine Similarity, which better captures structural relationships
Thresholding Technique	Applies Hard Thresholding in the basic step	Applies Soft Thresholding with Adaptive Thresholding based on noise levels
Filtering Mechanism	Two-step filtering: Hard Thresholding followed by Wiener Filtering	Enhanced two-step filtering: Soft Thresholding (adaptive) followed by Wiener Filtering
Final Reconstruction	Aggregation by weighted averaging using fixed weights	Aggregation with adaptive weights based on local variance of block estimates
Noise Adaptability	Less robust to varying noise levels	Highly adaptable to varying noise levels through adaptive thresholding
Preservation of Detail	Moderate preservation of image details (may blur edges/textures)	Superior preservation of textures and structural details

is further refined using Wiener filtering in the final stage to yield the final denoised output. While BM3D is effective in many denoising tasks, it suffers from certain drawbacks, particularly in balancing noise suppression with the preservation of essential image features such as edges and textures. These limitations primarily stem from the use of the Euclidean distance for block matching and the application of a fixed hard threshold for noise removal. Table 1 highlights the key differences between BM3D and the proposed CA-BM3D in terms of block matching, thresholding, and final reconstruction.

4.1. Innovations in CA-BM3D

The proposed CA-BM3D algorithm introduces two significant improvements:

- ***Cosine Similarity for Block Matching***: Unlike Euclidean distance, cosine similarity considers the angular similarity between vectors, thus capturing structural relationships more effectively [22]. This enhances the accuracy of block grouping, especially in the presence of high-frequency noise.
- ***Adaptive Soft Thresholding***: Replacing hard thresholding with adaptive soft thresholding enables CA-BM3D to adjust the threshold dynamically based on local noise levels and image characteristics, preserving fine details while effectively removing noise.

These modifications allow CA-BM3D to outperform traditional BM3D, particularly in terms of denoising accuracy and feature retention.

4.2. Overview of the BM3D algorithm

The BM3D algorithm consists of the following stages as illustrated in Fig. 1:

1) ***Block Partitioning***: The image is divided into overlapping patches of fixed size.
2) ***Block Matching***: For each reference block, similar blocks are identified across the image using Euclidean distance.
3) ***Collaborative Filtering***: Groups of similar patches are stacked into a 3D array and subjected to hard thresholding in the transform domain.
4) ***Aggregation***: Inverse transform is applied, and estimates from overlapping blocks are aggregated via weighted averaging to reconstruct the denoised image.

4.3. Comparative explanation of thresholding mechanisms in BM3D and CA-BM3D

A. Thresholding Mechanisms in BM3D

In the original BM3D framework, thresholding plays a crucial role in denoising grouped similar blocks after 3D transformation. Two conventional approaches are employed:

- ***Hard Thresholding (HT)*:** Applied in the basic estimation step, this method eliminates coefficients below a predefined global threshold. While it effectively removes noise, it may also suppress subtle image details, leading to a loss of texture and fine structures.
- ***Soft Thresholding (ST)*:** Typically used in the final Wiener filtering step, soft thresholding attenuates rather than completely discards coefficients, reducing artifacts but still relying on a fixed threshold, which may not perform optimally under varying noise levels or across image regions with diverse texture characteristics.

B. Proposed Adaptive Thresholding in CA-BM3D

The adaptive thresholding mechanism in CA-BM3D introduces a dynamic, data-driven approach that tailors the threshold value based on local noise variance and block activity. This innovation is

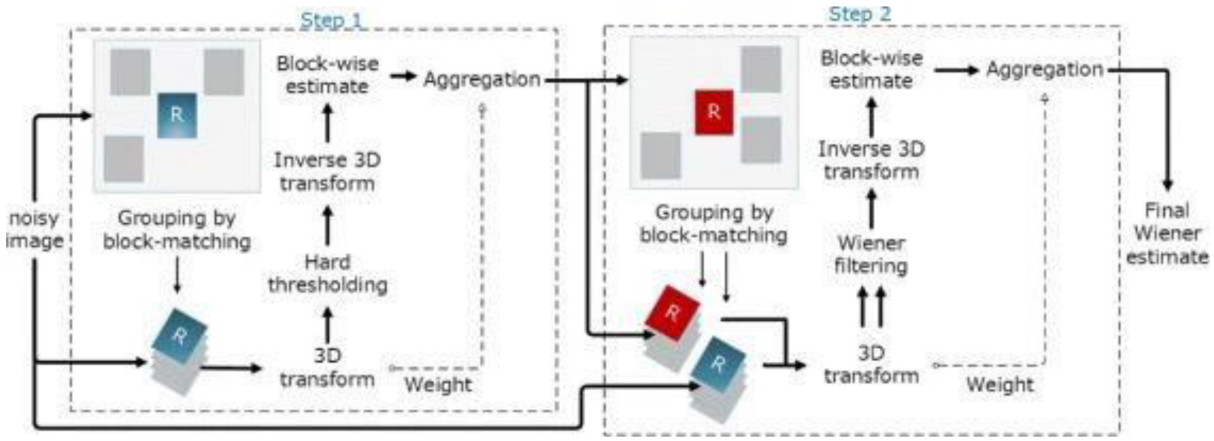

Fig. 1. Block diagram steps in the BM3D algorithm.

Table 2. Key differences of traditional HT/ST in BM3D and adaptive thresholding in CA-BM3D.

Aspect	Traditional HT/ST in BM3D	Adaptive Thresholding in CA-BM3D
Threshold Type	Fixed threshold for the entire image	Threshold computed dynamically per block group
Noise Sensitivity	Weak adaptability to noise variance	Highly sensitive to local noise statistics
Detail Preservation	Tends to smooth textures and suppress weak edges	Preserves edges and fine textures while suppressing noise
Computation Basis	Empirical or pre-defined threshold	Based on local variance and signal-to-noise ratio (SNR)
Denoising Performance	May underperform in high-frequency regions	Superior performance across both smooth and textured areas

rooted in the observation that noise is not uniformly distributed, especially in real-world scenarios. Key differences are shown in Table 2.

4.4. Proposed CA-BM3D algorithm architecture

The CA-BM3D algorithm comprises two sequential stages: basic estimation and final estimation, as depicted in Fig. 2.

A. **Basic Estimation Stage**

This stage involves the following key steps:

(a) ***Block Partitioning*:** The noisy image is divided into overlapping patches. Each patch serves as a reference block for matching.

(b) ***Block Matching with Cosine Similarity*:** Unlike BM3D, CA-BM3D utilizes cosine similarity to measure similarity between blocks. Cosine similarity is calculated as:

$$\cos(\theta) = \frac{x.y}{\|x\|\,\|y\|} \tag{1}$$

Where x and y are vectorized image blocks. This allows the algorithm to form 3D groups with structurally similar patches more effectively.

(c) ***Adaptive Soft Thresholding (Adaptive Filtering)*:** CA-BM3D replaces fixed hard thresholding with adaptive soft thresholding, defined as:

$$ST = \begin{cases} \text{sign}(Y)(|Y| - \tau), & \text{if } |Y| > \tau \\ 0, & \text{if } Y < \tau \end{cases} \tag{2}$$

Where Y is the transformed coefficient and τ is the adaptive threshold computed as:

$$\tau = \frac{\sigma^2}{\sigma_n^2} \tag{3}$$

Here, σ^2 is the clean signal variance and σ_n^2 is the noise variance. This allows thresholding to adapt to local noise characteristics.

(d) ***Inverse 3D Transform and Aggregation*:** The denoised coefficients are transformed back to the spatial domain using inverse 3D transformation. Aggregation is performed by weighted averaging of overlapping block estimates, where weights are inversely proportional to the sample variance.

B. **Final Estimation Stage**

This stage refines the initial estimate using Wiener Collaborative Filtering. The procedure is:

1) ***Block Matching*** is repeated as in the basic step.

2) ***Wiener Filtering*** is applied by computing shrinkage coefficients from the basic estimate and applying them to the grouped noisy patches.
3) ***Inverse 3D Transformation and Aggregation*** yield the final denoised image.

Wiener filtering in this context enhances detail preservation while reducing residual noise.

5. Results and discussion

5.1. Experimental setup

The experiment's primary objective is to demonstrate the proposed technique's performance and effectiveness in removing noise and preserving an image's features, such as lines, edges, and textures. The performance measure is evaluated by changing the noise levels from 10 to 40 db and by varying methods for distance measures while finding similar patches in block matching. The images of six benchmark datasets are taken, and five different distance metrics are applied to noise removal. The results are obtained by executing the CA-BM3D with different distance measures.

5.2. Dataset description

The proposed algorithm is implemented in Python Anaconda. Our proposed CA-BM3D is applied to six different 8-bit grayscale images such as Leena (512*512), Barbara (512*512), Zelda (512*512), peppers (512*512), Cameraman (512*512), House (512*512). All six datasets with additive white Gaussian noise, and five different distance measures are denoised, such as Euclidean distance, cosine distance, Minkowski distance, Jaccard distance, and Manhattan distance, are applied and implemented to estimate the performance of our proposed algorithm. The image datasets are shown in Fig. 3. Peak Signal to Noise Ratio and SSIM are applied as the evaluation criteria to compare the performance of the proposed technique.

To validate the performance of proposed technique, the denoised image is evaluated with specific evaluation criterion [23]. To compare proposed algorithm with all the other distance measures quantitatively, the Peak Signal to Noise Ratio (PSNR) index [24] and the Structural Similarity (SSIM) index [25] are calculated. PSNR accurately describes the similarity

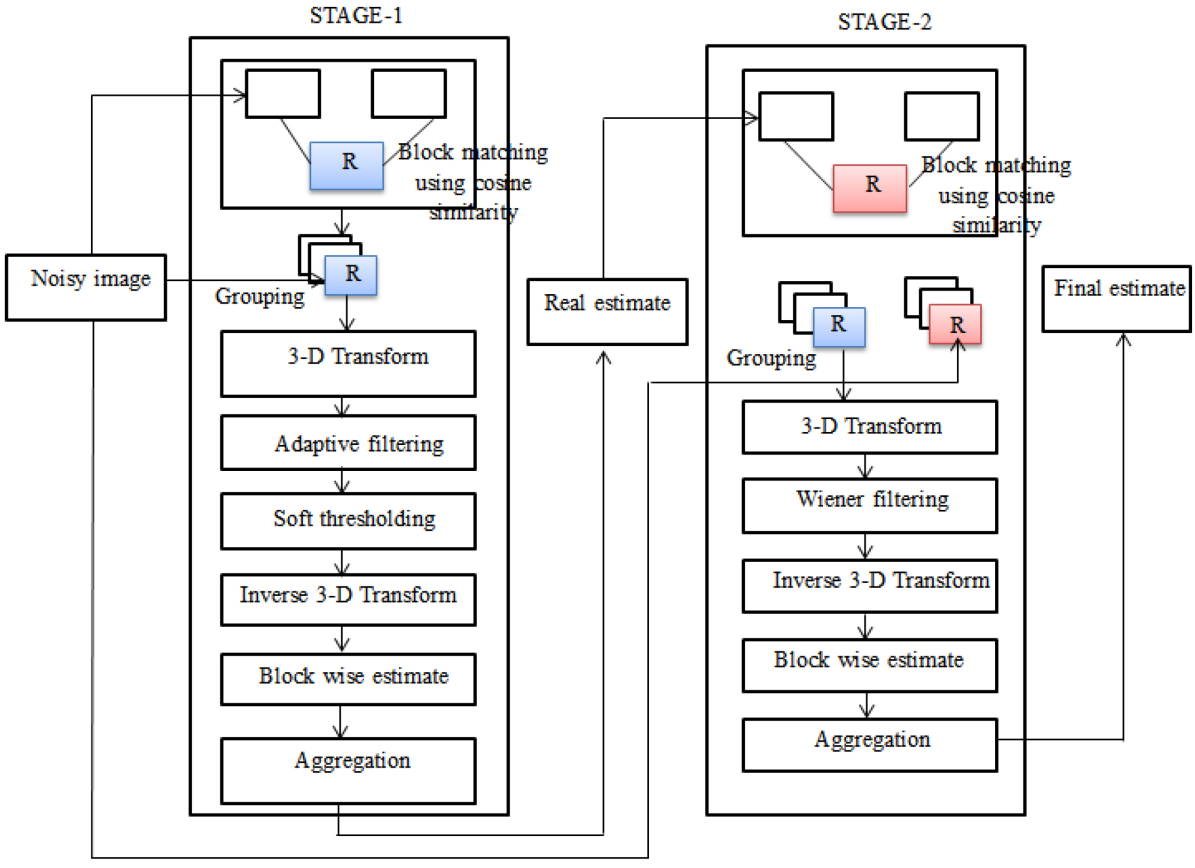

Fig. 2. Block diagram steps in the CA-BM3D algorithm.

Two-Stage Image Denoising Algorithm (CA-BM3D with Cosine Similarity)

Input: Noisy image
Output: Final denoised image
Stage 1: Initial Estimate

- **Block Matching (using Cosine Similarity)**
  - Divide the noisy image into reference blocks.
  - For each reference block, find similar blocks based on cosine similarity.
  - Group these similar blocks to form 3D groups.
- **Grouping**
  - Stack the matched blocks into a 3D array for collaborative filtering.
- **3-D Transform**
  - Apply a 3D transformation (e.g., DCT or Wavelet Transform) to the group.
- **Adaptive Filtering**
  - Apply filtering tailored to the noise characteristics.
- **Soft Thresholding**
  - Suppress noise by applying soft thresholding in the transform domain.
- **Inverse 3-D Transform**
  - Apply the inverse of the 3D transform to return to the spatial domain.
- **Block-wise Estimate**
  - Reconstruct denoised blocks from inverse-transformed data.
- **Aggregation**
  - Aggregate the overlapping block-wise estimates into a real estimate of the image.

Stage 2: Final Estimate (Refinement)

9. **Block Matching (again using Cosine Similarity)**
   - Use the **real estimate** from Stage 1 as guidance for new block matching.
   - Again group similar blocks using cosine similarity.
10. **Grouping**
    - Form updated 3D groups from both the noisy image and the real estimate.
11. **3-D Transform**
    - Apply a 3D transformation to these new 3D groups.
12. **Wiener Filtering**
    - Perform Wiener filtering using the real estimate as a reference.
13. **Inverse 3-D Transform**
    - Return the filtered blocks to the spatial domain.
14. **Block-wise Estimate**
    - Obtain refined denoised blocks.
15. **Aggregation**
    - Aggregate all refined block-wise estimates into the final denoised image.

between the original image and the denoised image. PSNR computes the peak signal-to-noise ratio in decibels (in dB) between original and denoised images. The computed ratio compares the quality of an original and a denoised image. The higher the PSNR measure, the higher the quality of the denoised or rebuilt image. PSNR is calculated as follows:

$$\mathrm{PSNR} = 10\log\frac{255 * 255 * P_x * P_y}{\sum_{i=1}^{P_x}\sum_{j=1}^{P_y}[I_{de}(i,j) - I_{or}(i,j)]^2} \quad (4)$$

Fig. 3. The grayscale 512* 512 image datasets were taken for analysis. From top to bottom and from left to right: the original image of Barbara, Cameraman, House, peppers, Leena, and Zelda.

Where P_x and P_y are the numbers of pixels vertically and horizontally, and $I_{de}(i, j)$ and $I_{or}(i, j)$ are the denoised and original images, respectively. The higher PSNR illustrates the higher quality of the extracted image.

5.3. Results and interpretation

To validate the effectiveness of the proposed algorithm CA-BM3D, the PSNR index was evaluated and compared by deploying different distance metrics such as Euclidean distance, Minkowski distance, Jaccard distance, Manhattan distance and proposed cosine distance metrics across different images like Leena, Barbara, Zelda, peppers, Cameraman, and House. Fig. 4 presents the PSNR performance of the different approaches across increasing standard deviation for the Leena image. On average, when the standard deviation increased, other distance metrics mentioned above incurred average PSNR, while the, proposed cosine distance achieved a better PSNR. This illustrates that the proposed denoising method ensures the image's better quality. Consequently, the PSNR was evaluated for the cameraman image for different distance metrics for the Zelda image across varying standard deviations from 10 to 40. The proposed algorithm achieved a higher PSNR of 32.2485, highlighting its reliability in producing an exact image as the original image with lower noise content. Fig. 5 provides the comparison of the PSNR of the proposed with different distance metrics for the Zelda image across varying standard deviations.

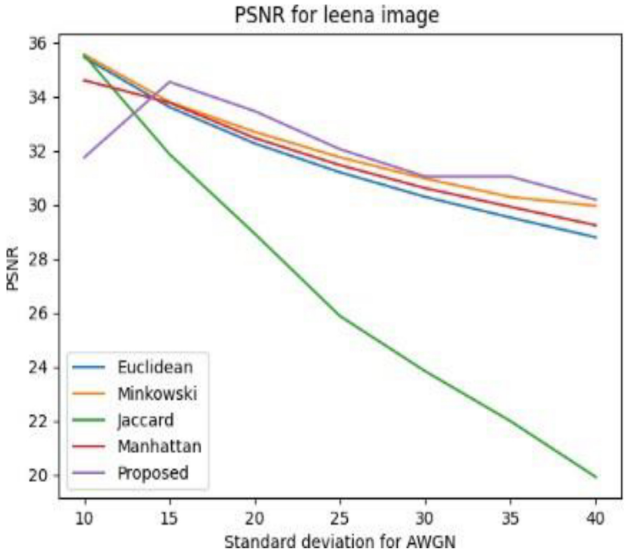

Fig. 4. Comparison of PSNR of different distance metrics with AWGN for Leena.

On the other hand, for Barbara's image, the PSNR of the proposed algorithm was determined and validated with other distance metrics like Euclidean distance, Minkowski distance, Jaccard distance, and Manhattan distance. Fig. 6 depicts the comparison of PSNR of different distance metrics with AWGN for Barbara's image. The CA-BM3D with other distance metrics achieved an average PSNR of 29.7816, 22.2997, 26.5524, and 28.7242, respectively. However, the proposed algorithm significantly improved the PSNR value (28.8304). This demonstrates that this strategy is more efficient

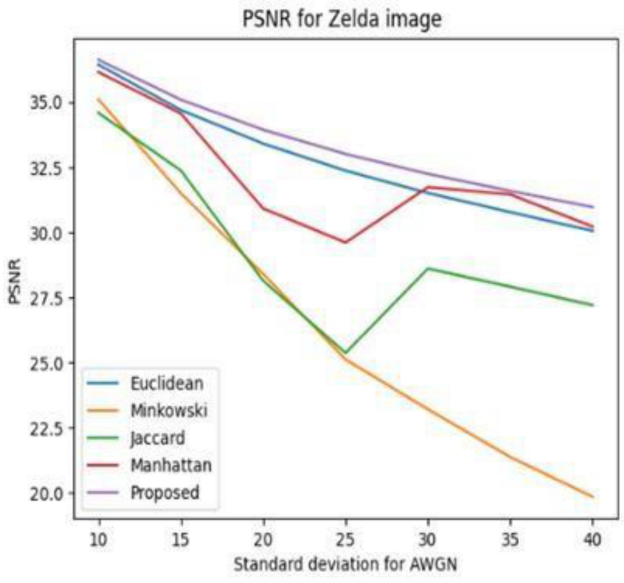

Fig. 5. Comparison of PSNR of different distance metrics with AWGN for Zelda image.

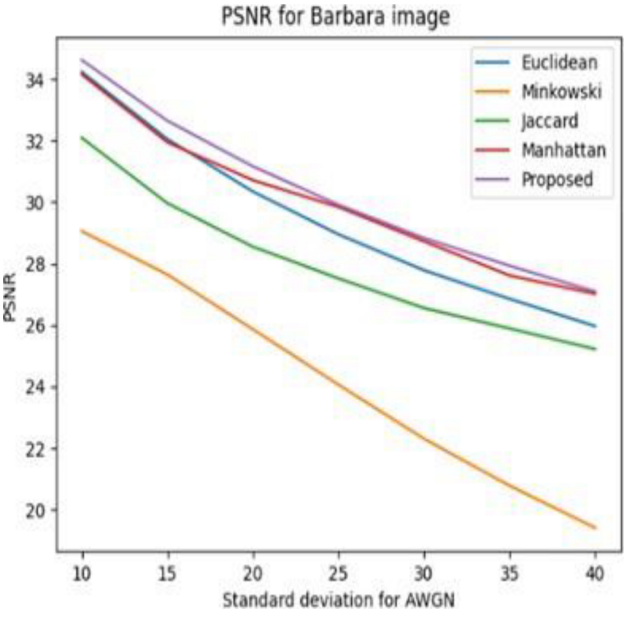

Fig. 6. Comparison of PSNR of different distance metrics with AWGN for Barbara's image.

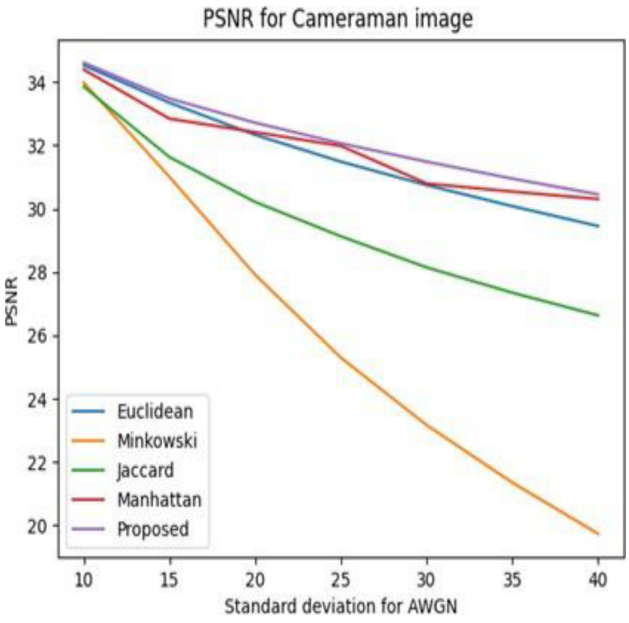

Fig. 7. Comparison of PSNR of different distance metrics with AWGN for Cameraman image.

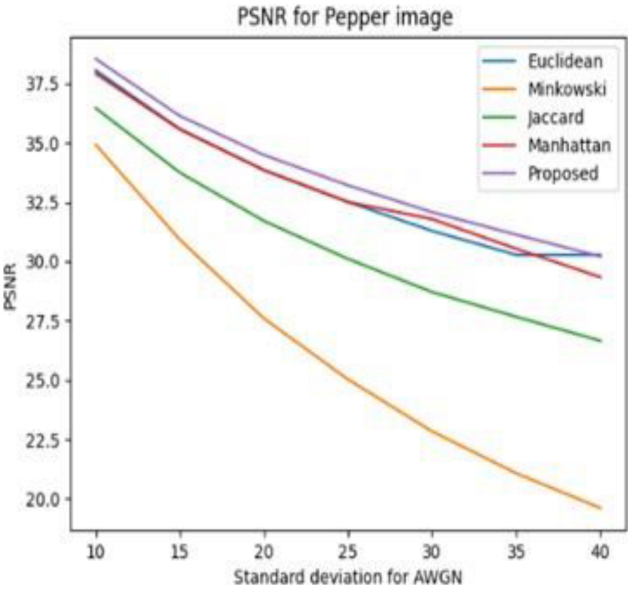

Fig. 8. Comparison of PSNR of different distance metrics with AWGN for Peppers image.

in removing image noise features. Consequently, the PSNR performance was determined for cameraman images for different distance metrics at varying standard deviations. Fig. 7 presents the comparative analysis of PSNR performance of CA-BM3D with different distance metrics across varying standard deviations. On average, other distance metrics, including Euclidean distance, Minkowski distance, Jaccard distance, and Manhattan distance, obtained PSNR of 30.7477, 23.1674, 28.1478, and 30.7985, respectively, while the proposed algorithm achieved better PSNR of 31.4876. This demonstrates that the proposed methodology provides images of better quality than other distance measures.

Fig. 8 depicts the comparative evaluation of PSNR of different distance metrics with varying standard deviations for the peppers image. The CA-BM3D with distance metrics including Euclidean distance, Minkowski distance, Jaccard distance, and Manhattan distance obtained PSNR of 31.2852, 22.837,

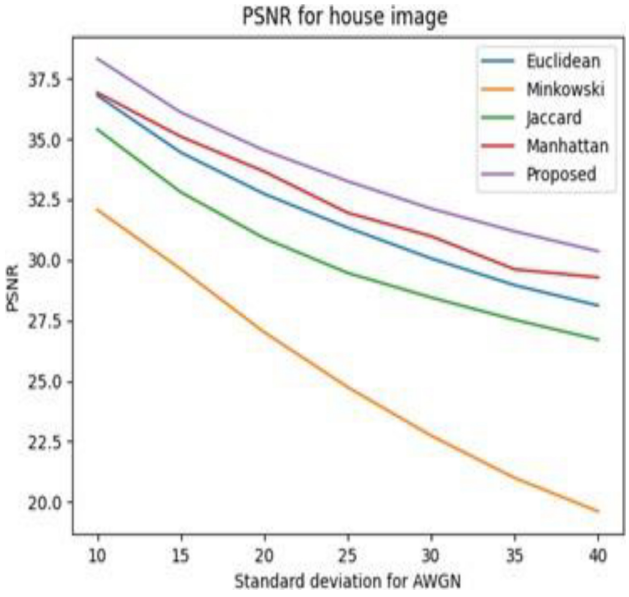

Fig. 9. Comparison of PSNR of different distance metrics with AWGN for house image.

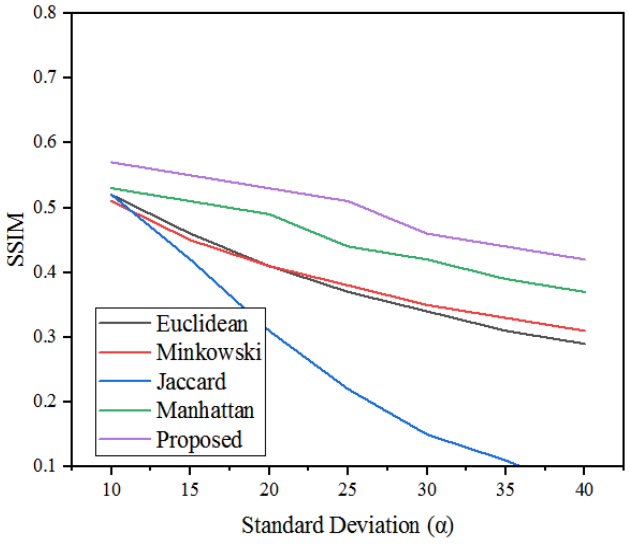

Fig. 10. SSIM graph of BM3D algorithm with different distance metrics for Leena.

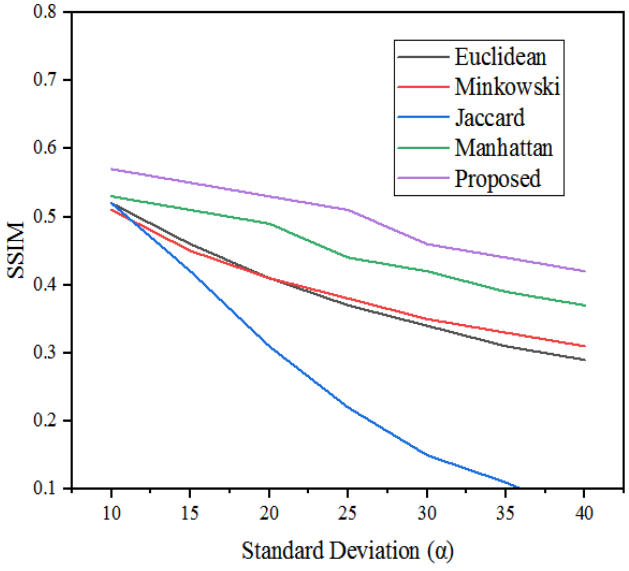

Fig. 11. SSIM graph of proposed algorithm with different distance metrics for Zelda.

28.7083, and 31.7826, respectively. However, the proposed strategy earned a higher PSNR of 32.0737, which illustrates that it precisely identifies and removes the noisy features from the image. Finally, the PSNR was estimated for the house image, and the comparative assessment is depicted in Fig. 9. The CA-BM3D with common distance metrics obtained PSNR of 30.67, 22.7365, 28.4506, and 30.9851, respectively. The proposed model achieved a better PSNR of 31.1857, which depicts the model's effectiveness in denoising the image. This intensive evaluation of the PSNR of the proposed CA-BM3D with deploying five common distances metrics in block matching demonstrated that the proposed model produced better PSNR than the existing distance metrics. These outcomes show that optimal PSNR is achieved for our proposed model among all other models for Barbara, Cameraman, House, peppers, Leena, and Zelda images. Our proposed algorithm gains more than 0.55 dB, which is higher than other algorithms with different distance metrics.

The Structural Similarity (SSIM) index is a method for evaluating how similar two images are. The SSIM index is a quality measure of the images being compared, assuming that one of the images is of perfect quality. SSIM is calculated as follows:

$$\mathrm{SSIM}(x) = \frac{(2\mu_x\mu_y + C_1)(2\sigma_{xy} + C_2)}{(\mu_x^2 + \mu_y^2 + C_1)(\sigma_x^2 + \sigma_y^2 + C_2)} \quad (5)$$

Where original image and denoised image are represented by x and y, μ_x and μ_y are the average gray values of the original and denoised results obtained, σ_x^2 and σ_y^2 represents the variances of original image and the denoised image, $\mu_x\mu_y$ represents the covariance between the original and the denoised image respectively and C_1, C_2 are the constants. The metric measures the image quality degradation caused by the denoising mechanism. Figs. 3 to 15 compares our proposed CA-BM3D model algorithm deploying common distance metrics like Euclidean distance, Minkowski distance, Jaccard distance, and Manhattan distance. For six images: Barbara, Cameraman, House, Peppers, Zelda, and Leena. It can be observed that the SSIM of the proposed CA-BM3D algorithm

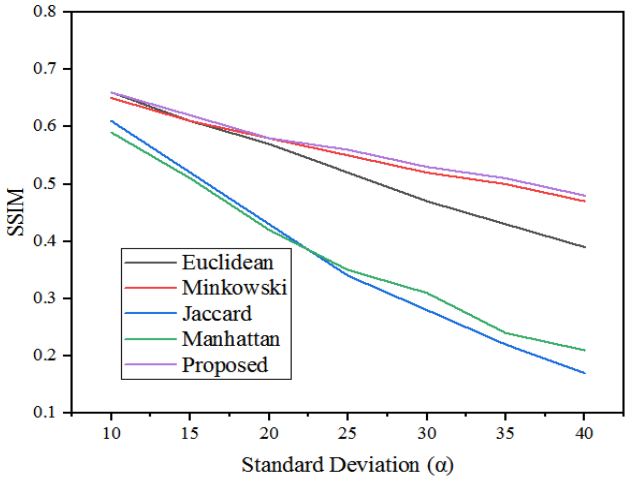

Fig. 12. SSIM graph of proposed algorithm with different distance metrics for Barbara.

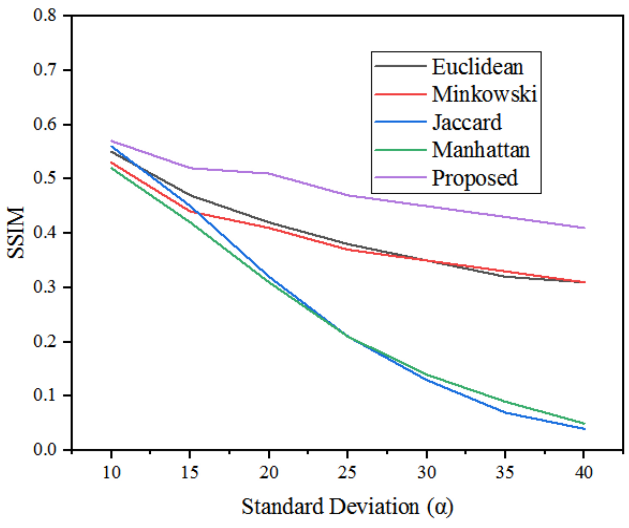

Fig. 13. SSIM graph of proposed algorithm with different distance metrics for Cameraman.

performs best at various Gaussian noise levels from $\alpha = 10$–40.

For the Leena image, the proposed algorithm achieved an average SSIM index of 0.46 ($\alpha = 30$). On the other hand, other distance metrics like Euclidean distance, Minkowski distance, Jaccard distance, and Manhattan achieved SSIM values of 0.34, 0.35, 0.15, and 0.42, respectively. Fig. 10 presents the SSIM analysis for the Leena image. Consequently, the SSIM was analyzed for the Zelda image, and it is observed that the proposed model obtained a higher SSIM index compared to others. It earned an SSIM of 0.46, which is relatively greater than the SSIM achieved by the above-mentioned distance metrics like Euclidean distance, Minkowski distance, Jaccard distance, and Manhattan. Fig. 11 presents the SSIM analysis for

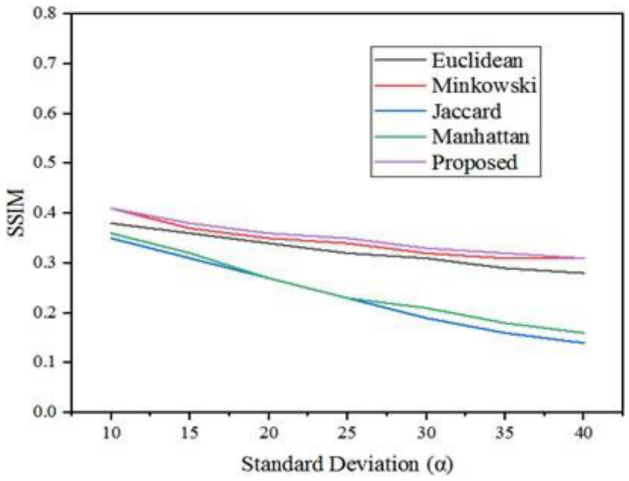

Fig. 14. SSIM graph of CA-BM3D algorithm with different distance metrics for House.

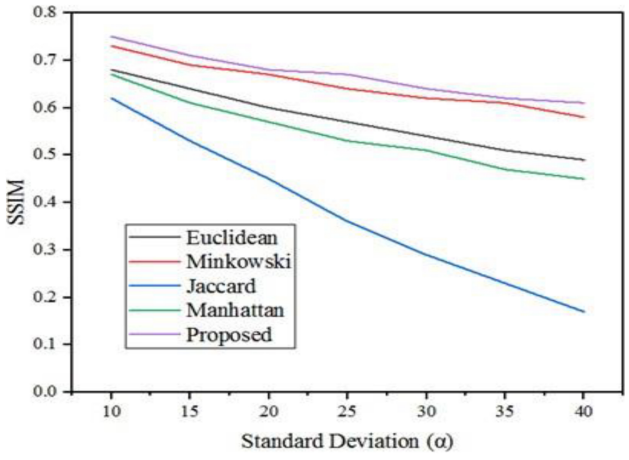

Fig. 15. SSIM graph of CA-BM3D algorithm with different distance metrics for Peppers.

the Zelda image. Subsequently, the SSIM index was determined for the CA-BM3D algorithm with different distance metrics for the Barbara image to validate the proposed models' efficiency in preserving the image quality and content while denoising operation. Fig. 12 depicts the comparative evaluation of the SSIM index. Fig. 13 illustrates the SSIM index for the Cameraman image of proposed method with different distance metrics. On average, these models achieved an SSIM index of 0.35, 0.35, 0.13, and 0.14, respectively, while the proposed distance metric earned an SSIM index of 0.45. The significant improvement of the SSIM index depicts the model's effectiveness in preserving the structural features.

Fig. 14 presents the SSIM index for house image. On average, the CA-BM3D with distance metrics, including Euclidean distance, Minkowski distance, Jaccard distance, and Manhattan, achieved an SSIM index of

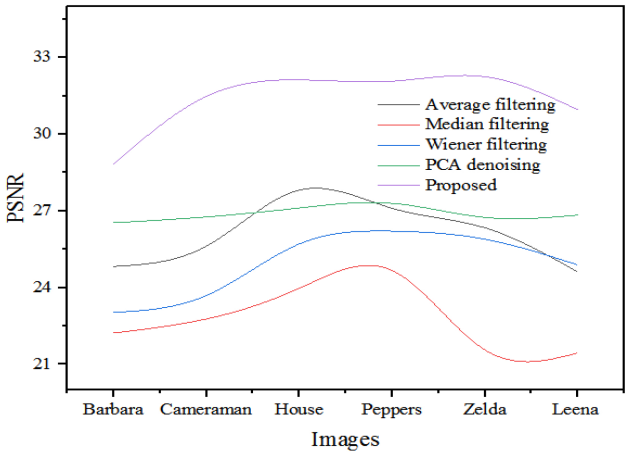

Fig. 16. Comparison of PSNR value in dB with Gaussian noise added (α = 30).

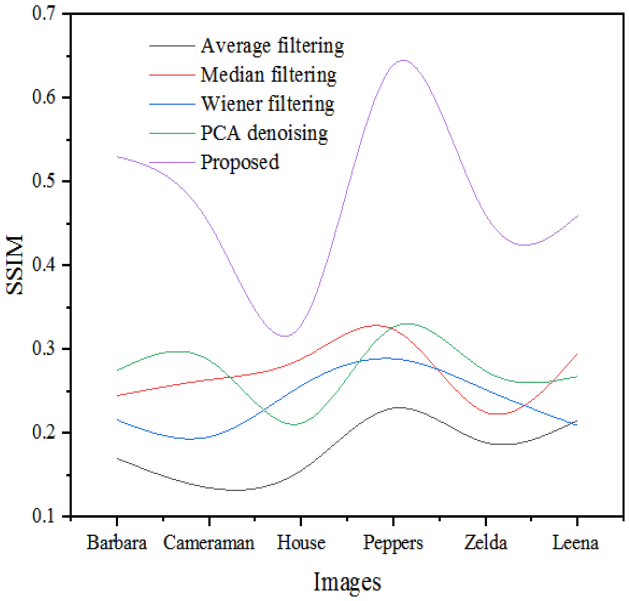

Fig. 17. Comparison of PSNR value in dB with Gaussian noise added (α = 30).

0.31, 0.32, 0.19, and 0.21, respectively. In contrast, the proposed distance metric earned an SSIM index of 0.33. The significant improvement of the SSIM index depicts the model's effectiveness in preserving the structural features. Finally, the SSIM index was evaluated for peppers by adding the Gaussian noise. The different distance metrics like Euclidean distance, Minkowski distance, Jaccard distance, and Manhattan obtained SSIM index of 0.54, 0.62, 0.29, and 0.51, while the proposed one obtained higher SSIM index of 0.63, which depicts the model's effectiveness in preserving the structural features of the original image. From this intensive evaluation, it is evident that the proposed model earned a better SSIM index compared to others. Fig. 15 presents the comparison of SSIM of CA-BM3D with different distance metrics with AWGN for pepper image.

Here, metrics like PSNR and SSIM are assessed for existing and proposed algorithms for different images, including Barbara, Cameraman, House, peppers, Zelda, and Leena images with Gaussian noise added (α = 30). The existing algorithms used include average filtering [32], median filtering [33], wiener filtering [34], and principal component analysis (PCA) denoising [35]. Fig. 16 compares the PSNR of the existing denoising algorithms. From the comparative assessment, it is evident that the proposed algorithm achieved improved PSNR for all six images, which highlights its effectiveness in preserving the original image features with fewer noise attributes. Fig. 17 depicts the comparative evaluation of the SSIM index with Gaussian noise added (α = 30). In this analysis, the SSIM index was assessed for six different images, and it is observed that the proposed algorithm comparatively achieved an increased SSIM index than the existing denoising models. This illustrates its efficiency in preserving the structural similarities in the images while reducing or removing the noise contents.

Table 3. Comparison study with other existing models based on PSNR.

Noise level	CA-BM3D	BM3D	Median Filter	Wavelet
10	31.28	29.54	28.90	27.65
15	29.85	27.75	27.10	26.98
20	28.45	26.55	26	25.20
30	26.10	24.85	24	23.55
40	24.25	23.15	22.85	22.25

Table 3 compares the performances of the existing denoising models with proposed method in terms of PSNR. The table gives the average PSNR of Leena, Barbara, house, pepper, cameraman images under various noise levels. PSNR is a very common metric to quantify the quality of the image resulting from any denoising process, where a higher value quantifies the better removal of noise with the preservation of finer image details. CA-BM3D outperforms the other techniques for all noise levels and images, considering that higher PSNR values are associated with better filtering. For example, at a noise level of 10, the PSNR obtained with CA-BM3D was 31.28 dB; meanwhile, for BM3D, the PSNR was 29.54 dB, Median Filter reached 28.90 dB, and Wavelet Denoising reached 27.65 dB. This order is maintained even at the noise level of 40 where CA-BM3D offers the value of 24.25 dB in comparison with 23.15 dB offered by BM3D. So, it clearly depicts how the proposed algorithm can be quite robust at high noise levels and possesses better image quality. Table 4 presents the comparison

Table 4. Comparison study with other existing models based on SSIM.

Noise level	CA-BM3D	BM3D	Median Filter	Wavelet
10	0.678	0.632	0.605	0.590
15	0.652	0.610	0.585	0.570
22	0.628	0.588	0.562	0.550
30	0.598	0.560	0.532	0.515
40	0.565	0.528	0.510	0.485

Table 5. Comparison study with other existing models based on MSE.

Noise level	CA-BM3D	BM3D	Median Filter	Wavelet
10	85.30	102.15	108.65	115
15	105.55	128.65	135.45	139.75
20	128.90	148.95	155.50	165.45
30	165.35	190.50	198	210.65
40	208.70	228.25	240.10	252.80

with respect to SSIM, which estimates the perceived similarity between denoised and original images. The table gives the average SSIM of Leena, Barbara, house, pepper, cameraman images under various noise levels .Higher values of SSIM are close to 1, and they imply higher structural fidelity. Similar to PSNR, CA-BM3D dominated the other models, especially for lower noise levels. For instance, CA-BM3D achieved an SSIM of 0.678 at a noise level of 10, while BM3D reached 0.632, Median Filter 0.605, and Wavelet Denoising 0.590. At a high noise level, such as 40, the SSIM of the proposed approach, while degraded, still stayed high at 0.565 compared to that of the other models, indicating better preservation of structural details according to the methodology when tested under conditions of higher noise.

Table 5 compares the MSE, which measures the difference between the denoised image and the original image. The table gives the average MSE of Leena, Barbara, house, pepper, cameraman images under various noise levels The lower the value of MSE is, the better the denoising performance will be. For all tested images and variation of noise level, CA-BM3D always provided the lowest MSEs. For example, for a noise level of 10, MSE for CA-BM3D is 85.30 and that for BM3D is 102.15, Median Filter is 108.65, and Wavelet Denoising is 115. It goes on widening with the noise level; the error rates are lower in the case of CA-BM3D. This means that the most contributions to noise reduction without sacrificing image quality are from adaptive thresholding and cosine similarity measures in CA-BM3D. As shown in Table 6, evaluation based on processing time of the models. The table gives the average processing time of Leena, Barbara, house, pepper, cameraman images under various noise levels This shows the fact that CA-BMD is computationally efficient. It requires less time for

Table 6. Comparison study with other existing models based on processing time (s).

Noise level	CA-BM3D	BM3D	Median Filter	Wavelet
10	0.85	1.50	0.98	1.05
15	0.90	1.60	1.10	1.12
20	1.15	1.80	1.25	1.25
30	1.35	2.05	1.50	1.40
40	1.60	2.25	1.75	1.58

processing in comparison with the BM3D algorithm. For instance, at noise level of 10, the CA-BM3D took 0.85 seconds which is very short compared to that of the BM3D, 1.50 seconds. Even at 75 dB noise levels, CA-BM3D processed within 1.60 seconds. BM3D took 2.25 seconds. Although CA-BM3D has certain cases where it takes more time to process as compared to Median Filter and Wavelet Denoising methods, the results based on PSNR, SSIM, and MSE are superior, hence compensating for the minimal increase in computation time. One of the major assets of CA-BM3D is that it balances computational efficiency with good quality of denoising.

6. Conclusion

This paper proposes a novel image denoising approach, the CA-BM3D algorithm, which enhances the performance of the standard BM3D method by replacing traditional Euclidean distance-based block matching with a cosine similarity measure and by incorporating a flexible adaptive thresholding mechanism in place of fixed hard thresholding. This innovative combination enables more accurate matching of similar image blocks and allows the algorithm to adapt its filtering strength to the characteristics of the noise, resulting in superior preservation of important image details such as edges and textures while effectively suppressing noise. The proposed method was evaluated using benchmark image datasets corrupted with AWGN and assessed through widely recognized image quality metrics like PSNR and SSIM. Experimental results demonstrate that CA-BM3D achieves an average PSNR of 31.28 and an SSIM of 0.678, outperforming traditional BM3D by delivering improved noise reduction and detail retention. These findings underscore the method's potential for real-world applications where both denoising and fidelity are critical. The algorithm is particularly well-suited for domains such as image processing and digital photography, where it enhances the visual quality of images captured under low-light or noisy conditions; medical imaging, where it aids in retaining diagnostically relevant structures in modalities like MRI, CT, and ultrasound;

remote sensing, where it refines satellite and aerial images distorted by atmospheric interference; and computer vision tasks such as object detection and facial recognition, where clean input images improve recognition accuracy. Additionally, CA-BM3D proves beneficial in video surveillance and real-time processing scenarios, ensuring edge and motion clarity across frames. The algorithm performs especially well on natural grayscale images characterized by complex textures and sharp structural features, and excels under AWGN, particularly at moderate to high noise levels. Overall, CA-BM3D emerges as a highly effective denoising solution capable of correcting the shortcomings of earlier methods, with strong prospects for broader applicability and real-time adaptation in diverse fields requiring high image fidelity and robust noise suppression.

Funding declaration

This research received no external funding.

Conflict of interest

The authors declare no conflict of interest.

Acknowledgment

I am grateful to all of those with whom I have had the pleasure to work during this and other related Research Work. Each of the members of my Dissertation Committee has provided me extensive personal and professional guidance and taught me a great deal about both scientific research and life in general.

References

1. Y. Guo, X. Zhou, J. Li, R. Ba, Z. Xu, S. Tu, and L. Chai, “A novel and optimized sine–cosine transform wavelet threshold denoising method based on the Sym4 basis function and adaptive threshold related to noise intensity,” *Appl. Sci.*, vol. 13, no. 19, 10789, 2023, doi: 10.3390/app131910789.
2. T. Rasal, T. Veerakumar, B. N. Subudhi, and S. Esakkirajan, “Fluorescence microscopy image noise reduction using IEMD-based adaptive thresholding approach,” *Signal Image Video Process.*, vol. 17, no. 1, pp. 237–245, 2023, doi: 10.1007/s11760-022-02226-y.
3. S. R. Thamanam, K. Manjunathachari, and K. S. Prasad, “An edge-preserving image denoising framework by adaptive thresholding-based DWT and modified deep structured architecture,” *Neural Process. Lett.*, vol. 55, no. 7, pp. 9353–9386, 2023, doi: 10.1007/s11063-023-11205-4.
4. Z. Lu, S. Jia, G. Li, and S. Jing, “Neutron image denoising method based on adaptive new wavelet threshold function,” *Nucl. Instrum. Methods Phys. Res. A*, vol. 1059, 169006, 2024, doi: 10.1016/j.nima.2023.169006.
5. N. Salamat, M. M. S. Missen, N. Akhtar, M. Mustahsan, and V. B. S. Prasath, “Color image restoration by filtering methods: A review,” *Soft Comput.*, vol. 28, no. 13, pp. 7755–7782, 2024, doi: 10.1007/s00500-024-09673-4.
6. E. Goceri, “Evaluation of denoising techniques to remove speckle and Gaussian noise from dermoscopy images,” *Comput. Biol. Med.*, vol. 152, 106474, 2023, doi: 10.1016/j.compbiomed.2022.106474.
7. H. Xu, X. Jia, L. Cheng, and H. Huang, “Affine non-local Bayesian image denoising algorithm,” *Vis. Comput.*, vol. 39, no. 1, pp. 99–118, 2023, doi: 10.1007/s00371-021-02316-x.
8. M. Elad, B. Kawar, and G. Vaksman, “Image denoising: The deep learning revolution and beyond—a survey paper,” *SIAM J. Imaging Sci.*, vol. 16, no. 3, pp. 1594–1654, 2023, doi: 10.1137/23M1545859.
9. C. Kong, W. Yu, Q. Zeng, Z. Chen, and Y. Peng, “A similarity-based remaining useful life prediction method using multimodal degradation features and adjusted cosine similarity,” *Meas. Sci. Technol.*, vol. 34, no. 10, 105112, 2023, doi: 10.1016/j.ymssp.2017.11.016.
10. M. Chen *et al.*, “Optimized variational mode decomposition algorithm based on adaptive thresholding method and improved whale optimization algorithm for denoising magnetocardiography signal,” *Biomed. Signal Process. Control*, vol. 88, 105681, 2024, doi: 10.1016/j.bspc.2023.105681.
11. D. Devapal, S. S. Kumar, and R. Sethunadh, “Discontinuity adaptive SAR image despeckling using curvelet-based BM3D technique,” *Int. J. Wavelets Multiresolut. Inf. Process.*, vol. 17, no. 03, 1950016, 2019, doi: 10.1142/S0219691319500164.
12. M. Hasan and M. R. El-Sakka, “Improved BM3D image denoising using SSIM-optimized Wiener filter,” *EURASIP J. Image Video Process.*, vol. 2018, no. 1, pp. 1–12, 2018, doi: 10.1186/s13640-018-0264-z.
13. C. Knaus and M. Zwicker, “Dual-domain filtering,” *SIAM J. Imaging Sci.*, vol. 8, no. 3, pp. 1396–1420, 2015, doi: 10.1137/140978879.
14. A. A. Yahya *et al.*, “BM3D image denoising algorithm based on an adaptive filtering,” *Multimed. Tools Appl.*, vol. 79, pp. 20391–20427, 2020, doi: 10.1007/s11042-020-08815-8.
15. R. Chen, D. Pu, Y. Tong, and M. Wu, “Image-denoising algorithm based on improved K-singular value decomposition and atom optimization,” *CAAI Trans. Intell. Technol.*, vol. 7, no. 1, pp. 117–127, 2022, doi: 10.1049/cit2.12044.
16. M. R. Rejeesh and P. M. O. T. F. Thejaswini, “MOTF: Multi-objective optimal trilateral filtering based partial moving frame algorithm for image denoising,” *Multimed. Tools Appl.*, vol. 79, no. 37, pp. 28411–28430, 2020, doi: 10.1007/s11042-020-09234-5.
17. Z. Li, H. Liu, L. Cheng, and X. Jia, “Image denoising algorithm based on gradient domain guided filtering and NSST,” *IEEE Access*, vol. 11, pp. 11923–11933, 2023, doi: 10.1109/ACCESS.2023.3242050.
18. H. Huang, C. Zhang, L. Zhao, S. Ding, H. Wang, H. Wu, “Self-supervised medical image denoising based on wista-net for human healthcare in metaverse,” *IEEE J. Biomed. Health Inform.*, 2023, doi: 10.1109/JBHI.2023.3278538.
19. H. Deng, G. Liu, and L. Zhou, “Ultrasonic logging image denoising algorithm based on variational Bayesian and sparse prior,” *J. Electron. Imaging*, vol. 32, no. 1, 013004, 2023, doi: 10.1117/1.JEI.32.1.013004.
20. K. Naveed, B. Shaukat, and N. ur Rehman, “Dual tree complex wavelet transform-based signal denoising method exploiting neighbourhood dependencies and goodness-of-fit test,” *R. Soc. Open Sci.*, vol. 5, no. 9, 180436, 2018, doi: 10.1098/rsos.180436.

21. G. Maheswari and S. Gopalakrishnan, “A smart multimodal framework based on squeeze excitation capsule network (SEC-Net) model for disease diagnosis using dissimilar medical images,” *Int. J. Inf. Technol.*, vol. 17, no. 1, pp. 49–67, 2025, doi: 10.1007/s41870-024-02136-x.
22. E. K. Ruby, G. Amirthayogam, G. Sasi, T. Chitra, A. Choubey, and S. Gopalakrishnan, “Advanced image processing techniques for automated detection of healthy and infected leaves in agricultural systems,” *Mesopotamian J. Comput. Sci.*, pp. 44–52, 2024, doi: 10.58496/MJCSC/2024/006.
23. J. Chen, Z. Zhu, H. Hu, L. Qiu, Z. Zheng, and L. Dong, “A novel adaptive group sparse representation model based on infrared image denoising for remote sensing application,” *Appl. Sci.*, vol. 13, no. 9, 5749, 2023, doi: 10.3390/app13095749.
24. L. El Bouny, M. Zouidine, K. Fakhar, and M. Khalil, “Wavelet-based denoising diffusion models for ECG signal enhancement,” in *Proc. 2024 IEEE 12th Int. Symp. Signal, Image, Video Commun. (ISIVC)*, pp. 1–5, 2024, doi: 10.1109/ISIVC61350.2024.10577937.
25. A. Annavarapu and S. Borra, “An adaptive watershed segmentation based medical image denoising using deep convolutional neural networks,” *Biomedical Signal Processing and Control*, 93, 106119, 2024, https://doi.org/10.1016/j.bspc.2024.106119